CHALMERS | UNIVERSITY OF GOTHENBURG

PREPRINT 2011:29

Adaptive Finite Element Method for the Fredholm Integral Equation of the First Kind and its Verification on the Experimental Data

N. KOSHEV
L. BEILINA

Department of Mathematical Sciences
Division of Mathematics
CHALMERS UNIVERSITY OF TECHNOLOGY
UNIVERSITY OF GOTHENBURG
Gothenburg Sweden 2011

Preprint 2011:29

Adaptive Finite Element Method for the Fredholm Integral Equation of the First Kind and its Verification on the Experimental Data

N. Koshev and L. Beilina

Department of Mathematical Sciences
Division of Mathematics
Chalmers University of Technology and University of Gothenburg
SE-412 96 Gothenburg, Sweden
Gothenburg, December 2011

Preprint 2011:29
ISSN 1652-9715

Matematiska vetenskaper
Göteborg 2011

ADAPTIVE FINITE ELEMENT METHOD FOR THE FREDHOLM INTEGRAL EQUATION OF THE FIRST KIND AND ITS VERIFICATION ON THE EXPERIMENTAL DATA

N.KOSHEV* AND L. BEILINA *,1

Abstract. We propose an adaptive finite element method for the solution of the linear Fredholm integral equation of the first kind. We derive a posteriori error estimate in the functional to be minimized. To do it we specify nonlinear results obtained in [9, 10, 11, 12, 16] for the case of the linear bounded operator. Accuracy of the regularized solution is also presented. Numerical experiments justify the efficiency of our a posteriori estimates applied both to the computationally simulated and experimental backscattered data measured in microtomography.

1. Introduction. In this work we consider a problem of the solution of the Fredholm integral equation of the first kind and propose at the first time an adaptive finite element method to solve it. Such problems arise in many applications of astrophysics [1], astronomy [2], image processing on the smeared and defocused photographies [4] and image processing in microtomography [5], spectroscopy in the backscattered electron signal [6], etc. In our consideration we specify results of [9, 10, 11, 12, 16] for the case of linear Fredholm integral equation which is ill-posed problem. Because of the linearity, results of this paper sound more clear than those of previous works and proofs here are different from ones of [9, 10, 11, 12, 16]. Another new element of this paper is that the Tikhonov regularization term is given in H^1 norm, which is stronger than the L_2 norm being used for the original operator of [9, 10, 11, 12, 16]. This causes certain additional difficulties, compared with [16], where the L_2 norm was used for both the original operator and the Tikhonov regularization term.

We note that in [9, 12] *a posteriori* error estimates were obtained not for the exact but for the regularized coefficient. In the follow-up work [16] the effort of the accuracy improvement of the regularized coefficient rather than the exact coefficient was explained. More precisely, from [16] follows that the regularized coefficient is closer to the exact coefficient than the first guess in the nonlinear case. Therefore, an improvement of the accuracy of the reconstruction of the regularized coefficient on the adaptively refined meshes leads to an improvement of the accuracy of the reconstruction of the exact solution. First, similarly with [9, 12] in our work we obtain a posteriori error estimates for the regularized function. Next, using results of [16] we show that the regularized function is closer to the exact function in the case of the bounded linear operator.

The main concept of the adaptivity technique, which we apply to the Fredholm integral equation of the first kind, is following. In the case of ill-posed problems it is inefficient to use an exceedingly fine mesh in computations. The main idea of the adaptive finite element method is to obtain a good accuracy of solutions via local mesh refinements. In order to do it, we minimize the Tikhonov functional on a sequence of locally refined meshes. A posteriori error analysis developed in this paper answers to the main question in the adaptivity: where locally refine the mesh to improve the resulting solution.

In our numerical examples we show efficiency of the adaptivity technique on image restoration problem arised in electron micsroscopy [4, 5]. The goal of our tests is to restore blurred images obtained in electron microscopy, and identify possible defects on them. To do that we apply adaptive algorithm of Section 6. Since in computational examples of Section 7 we work only with a finite dimensional space of standard piecewise linear finite elements, then we consider our problem in a finite dimensional space. However, the corresponding Fredholm equation operator certainly inherits the ill-posed nature of its infinitely dimensional analog. Therefore, it is worth to consider the Tikhonov functional.

In Tests 1,2 of Section 7 we applied computationally simulated data, while in Test 3 was used real measured backscattered data obtained by microtomograph developed by professor Eduard Rau at Moscow

*Department of Physics, Penza State University of Architecture and Building, Russian Federation, *email*: nikolay.koshev@gmail.com

*,1 Corresponding author, Department of Mathematical Sciences, Chalmers University of Technology and Gothenburg University, SE-42196 Gothenburg, Sweden, *email*: larisa@chalmers.se

Lomonosov State University [4, 5]. Conclusion from these tests is that the local adaptive mesh refinement algorithm can significantly improve contrast of the blurred images. Comparison with other techniques which are used for solution of such kind of problems is outside of this publication. We plan to consider it as future work. However, in Test 2 of Section 7 we compared performance of our adaptive algorithm with performance of methods of [5, 18] on reconstruction of deconvolution function. Our computational tests show the better stability of the adaptive method with respect to the regularization parameter then the stability of methods presented in [5, 18].

2. The Framework Of the Functional Analysis. We introduce first common notations which we are using in this paper. Let $\Omega \subset \mathbb{R}^n, n = 2, 3$ be a bounded domain with the piecewise-smooth boundary $\partial\Omega$. In our numerical experiments we are working with piecewise smooth boundaries and this is one of discrepancies between the theory and its numerical implementation.

Let function $u(x), x = (x_1, ..., x_n) \in \Omega$ be a k times continuously differentiable in Ω. We denote the partial derivative of the order $|\alpha| \leq k$, of function u by

$$D^\alpha u = \frac{\partial^{|\alpha|} u}{\partial^{\alpha_1} x_1 \dots \partial^{\alpha_n} x_n}, \ \ |\alpha| = \alpha_1 + \ldots + \alpha_n$$

where $\alpha = (\alpha_1, \ldots, \alpha_n)$ is such that $\alpha_i \geq 0$.

Denote $C^k\left(\overline{\Omega}\right)$ the Hilbert space of functions $u(x)$ which are continuous in the closure $\overline{\Omega}$ of the domain Ω together with their derivatives $D^\alpha u, |\alpha| \leq m$. The norm in this space is defined as

$$\|u\|_{C^k(\overline{\Omega})} = \sum_{|\alpha| \leq m} \sup_{x \in \Omega} |D^\alpha u(x)| < \infty.$$

Consider the Sobolev space $H^k(\Omega)$ of all functions with the norm defined as

$$\|u\|^2_{H^k(\Omega)} = \sum_{|\alpha| \leq k} \int\limits_\Omega |D^\alpha u|^2 \, dx < \infty,$$

where $D^\alpha u$ are weak derivatives of the function u.

$H^k(\Omega)$ is a Hilbert space with the inner product defined as

$$(u, v)_{H^k(\Omega)} = \sum_{|\alpha| \leq k} \int\limits_\Omega D^\alpha u D^\alpha v dx.$$

2.1. The finite element. Following [13] we call a triple (K, P_K, N_K) by a m-dimensional finite element where K is a closed bounded subset of $\mathbb{R}^m, m = 2, 3$ with nonempty interior and piecewise smooth boundary, P_K is a finite-dimensional vector space of functions defined on K, and N_K is a basis of the dual space P_K^* . The function space P_K is the space of the shape functions and the elements of N_K are the nodal variables or degrees of freedom. In this work as K we take triangle or tetrahedron in two and three space dimensions, respectively, P_K will be the space of piecewise linear functions and the set N_K will consist of evaluations of the shape functions at the vertices of triangles/tetrahedra. The dual basis of P_K we denote by $\varphi_1, ..., \varphi_n$, where $n = \dim P_K$, and nodal variables in N_K by $N_1, .., N_n$ such that

$$N_i(\varphi_j) = \delta_{ij} = \begin{cases} 1, & \text{if } i = j, \\ 0, & \text{if } i \neq j. \end{cases}$$

2.2. The space H of piecewise finite elements and its subspaces. Let $\Omega \subset \mathbb{R}^m, m = 2, 3$ be a bounded domain. We discretize the domain Ω by an unstructured mesh T using tetrahedral elements in $\mathbb{R}^3$ and triangles in $\mathbb{R}^2$. We define by T_0 the partition of this domain with a rather coarse mesh. Using subsequent mesh refinement procedure of the coarse mesh T_0 we obtain a new meshes with smaller mesh size.

Let T be one of those meshes. We approximate the function z on this triangulation by piecewise linear functions $\{\varphi_j(x)\}_{j=1}^n$ in a standard way [14] as $z(x) = \sum_{j=1}^n z_j \varphi_j(x)$ and thus construct a linear space of these functions.

Let h' be the diameter of triangles/tetrahedra in the element K of the mesh T and r' be the radius of the maximal circle/sphere contained in that triangle/tetrahedra. We make the following shape regularity assumption on the mesh T which means that we do not decrease the size of triangles/tetrahedra indefinitely

$$a_1 \leq h' \leq r' a_2; \quad a_1, a_2 = const. > 0. \tag{2.1}$$

From the above mesh regularity assumption follows that there exists only a finite number $\widetilde{N}$ of possible triangulations satisfying (2.1). Let us denote by $H = \cup_T Span(B(T))$. Thus H is a subspace of $L_2(\Omega)$ and $\dim H := d_H := d_H\left(\widetilde{N}\right) < \infty$. Furthermore,

$$H \subset \left(H^1(\Omega) \cap C\left(\overline{\Omega}\right)\right) \text{ as a set, } \partial_{x_i} f \in L_\infty(\Omega), \forall f \in H. \tag{2.2}$$

We denote by $(\cdot,\cdot)$ and $\|\cdot\|$ the scalar product and the corresponding norm in H, respectively. We consider the space H as an "ideal" space of very fine finite elements, which is never reached in computations.

We now construct subspaces $M_k \subset H$ associated with our triangulations T_k. These subspaces should be such that that

$$M_k \subset M_{k+1}. \tag{2.3}$$

The first coarse subspace we define by $M_0 := Span(B(T_0)) \subset H$. The next pair (T_{k+1}, M_{k+1}) for the given pair (T_k, M_k), is constructed in following way. We refine the mesh T_k and obtain the corresponding triangulation T_{k+1} and the corresponding basis $B(T_{k+1})$. Next, we define the space M_{k+1} as $M_{k+1} := Span(B(T_{k+1}))$. Since in approximation of our function $z(x)$ we use piecewise linear finite elements, $B(T_k) \subset Span(B(T_{k+1}))$. Hence, $Span(B(T_k)) := M_k \subset M_{k+1}$, i.e. (2.3) holds.

Let $P_M : H \to M$ for $\forall M \subset H$ be the operator of the orthogonal projection. To short notations we denote $P_k := P_{M_k}, P_{k+1} := P_{M_{k+1}}$. Let the function $f \in H^1(\Omega) \cap C\left(\overline{\Omega}\right)$ and its $\partial_{x_i} f_{x_i} \in L_\infty(\Omega)$.

Consider a mesh which is split into triangles/tetrahedral elements K such that $\overline{\Omega} = \cup \overline{K}$. In a general case we allow meshes in space with hanging nodes and assume that the local mesh size has bounded variation in such meshes. This means that there exists a constant $\gamma > 0$ such that $\gamma h_{K^+} \leq h_{K^-} \leq \gamma^{-1} h_{K^+}$ for all the neighboring elements K^- and K^+. We define also by h_K be the maximal diameter of the above triangles/tetrahedra which are involved in T_k. By the construction of above subspaces $h_{K+1} \leq h_K$.

Let S be the internal face of the non-empty intersection of the boundaries of two neighboring elements K^+ and K^-. We denote the jump of the function v_h computed from the two neighboring elements K^+ and K^- sharing the common side S as

$$[v_h] = v_h^+ - v_h^-. \tag{2.4}$$

We define by f_k^I the standard interpolant [14] on triangles/tetrahedra of the function $f \in H$. Then by one of properties of the orthogonal projection

$$\|f - P_k f\|_{L_2(\Omega)} \leq \left\|f - f_k^I\right\|_{L_2(\Omega)}. \tag{2.5}$$

Hence, it follows from (2.2, 2.5) and formula 76.3 of [14] that

$$\|f - P_k f\|_{L_2(\Omega)} \leq C_I \|\nabla f\|_{L_\infty(\Omega)} h_K, \forall f \in H. \tag{2.6}$$

where $C_I = C_I(\Omega)$ is positive interpolation constant depending only on the domain Ω.

2.3. Statement of the problem. Let H and L_2 be two Hilbert spaces and let $\Omega \subset \mathbb{R}^m, m = 2, 3$ be a convex bounded domain introduced in section 2.2.

Our goal is to solve the Fredholm integral equation of the first type

$$\int_\Omega \rho(x,y)z(x)dx = u(x), \tag{2.7}$$

where $u(x) \in L_2(\bar{\Omega})$, $z(x) \in H$, $\rho(x,y) \in C^k\left(\overline{\Omega} \times \overline{\Omega}\right), k \geq 0$ be the kernel of the integral equation.

For our next considerations we can rewrite (2.7) in an operator form as

$$A(z) = u \tag{2.8}$$

with an operator $A : H \to L_2(\bar{\Omega})$ defined as

$$A(z) := \int_\Omega \rho(x,y)z(x)dx. \tag{2.9}$$

Ill-posed problem.

Let the function $z(x) \in H$ of the equation (2.7) be unknown in the domain Ω. Determine the function $z(x)$ for $x \in \Omega$ assuming the functions $\rho(x,y) \in C^k\left(\overline{\Omega} \times \overline{\Omega}\right), k \geq 0$ and $u(x) \in L_2(\Omega)$ in (2.7) are known.

Although the function $A(z) \in C^k\left(\overline{\Omega}\right), k \geq 0$ we assume in (2.9) that $u \in L_2\left(\overline{\Omega}\right)$. The reason of this is that the right hand side of this equation can be given with a noise.

2.4. The Tikhonov functional. Let us assume that the right hand side of (2.7) is given with the small parameter $\delta \in (0,1)$ which characterizes the level of the error in data such that $u = u^* + \delta$. Let u^* be the ideal noiseless right hand side of (2.7) which corresponds to the ideal exact solution z^*,

$$A(z^*) = u^*, \quad \|u - u^*\|_{L_2(\Omega)} < \delta. \tag{2.10}$$

Let us consider all functions $z \in H$ and introduce the operator $F : H \to L_2$ such that

$$F(z) := Az - u. \tag{2.11}$$

Hence $Az^* - u^* = 0$ and thus $F(z^*) = Az^* - u = \delta$. We assume that

$$||F(z^*)||_{L_2(\Omega)} \leq \delta. \tag{2.12}$$

Although H is a finite dimensional space, where all norms are equivalent, we have discovered in our computations that it is better to use the $H^1(\Omega)$ norm in the regularizing term of the Tikhonov functional. Note that $H \subset H^1(\Omega)$ as a set.

To find an approximate solution of equation (2.7), we minimize the Tikhonov regularization functional $M_\alpha(z)$,

$$M_\alpha(z) = \frac{1}{2}\|F(z)\|^2_{L_2(\Omega)} + \frac{\alpha}{2}\|z - z_0\|^2_{H^1(\Omega)}, \tag{2.13}$$

$$M_\alpha : H \to \mathbb{R}, \quad z_0 \in H,$$

where $\alpha = \alpha(\delta) > 0$ is a regularization parameter which is small. How to choose the point z_0 depends on the concrete minimization problem. Usually z_0 is a good first approximation for the exact solution z^*.

Further, we consider more general form of the Tikhonov functional (2.13). Let W_1,W_2, Q be three Hilbert spaces, $Q \subseteq W_1$ as a set, the norm in Q is stronger than the norm in W_1 and $\overline{Q} = W_1$, where the closure is understood in the norm of W_1. We denote scalar products and norms in these spaces as

$$(\cdot,\cdot), \|\cdot\| \text{ for } W_1,$$

$$(\cdot,\cdot)_2, \|\cdot\|_2 \text{ for } W_2$$

$$\text{and } [\cdot,\cdot], [\cdot] \text{ for } Q.$$

Let $A : W_1 \to W_2$ be a bounded linear operator. Consider the general Tikhonov functional

$$J_\alpha(z) : Q \to \mathbb{R}, \tag{2.14}$$

$$J_\alpha(z) = \frac{1}{2}\|Az-u\|_2^2 + \frac{\alpha}{2}[z-z_0]^2, u \in W_2; z, z_0 \in Q, \tag{2.15}$$

where $\alpha \in (0,1)$ is the regularization parameter.

2.5. The Fréchet Derivative and the convexity of the Tikhonov Functional. The following lemma is well known [7]. Although some of its generalizations can also be formulated, we restrict our attention to the current one, since this is sufficient for our goal.

Lemma 1. *Let $A : W_1 \to W_2$ be a bounded linear operator. Then the Fréchet derivative of the functional (2.14) is*

$$J'_\alpha(z)(b) = (A^*Az - A^*u, b) + \alpha[z-z_0, b], \forall b \in Q. \tag{2.16}$$

In particular, for the integral operator (2.7) we have

$$J'_\alpha(z)(b) = \int_\Omega b(s)\left[\int_\Omega z(y)\left(\int_\Omega \rho(x,y)\rho(x,s)\,dx\right)dy - \int_\Omega \rho(x,s)u(x)\,dx\right]ds \tag{2.17}$$

$$+\alpha[z-z_0, b], \forall b \in Q.$$

Lemma 2 is also well known, since $A : W_1 \to W_2$ is a bounded linear operator. We again formulate this lemma only for our specific case, referring to [17] for a more general case. The situation is naturally more complicated for a nonlinear operator, and we refer to [9] for this case.

Lemma 2. *Let the operator $A : W_1 \to W_2$ satisfies conditions of Lemma 1. Then the functional $J_\alpha(z)$ is strongly convex on the space Q,*

$$(J'_\alpha(x) - J'_\alpha(z), x-z) \geq \alpha[x-z]^2, \forall x, z \in Q.$$

3. The accuracy of the regularized solution. In this section we specify results of [16] where only nonlinear operator was considered, for the case of the bounded linear operator. In Theorem 1 we recall proof of the existence and uniqueness of the minimizer z_α of the functional $J_\alpha(z)$. This theorem has been proved by A.N. Tikhonov. We establish this result for a bounded linear operator whose domain is the infinitely dimensional Hilbert space $L_2(\Omega)$. It is well known that z_α is called the *regularized solution.*

Theorem 1. *Let in (2.15) $A : W_1 \to W_2$ be a bounded linear operator. Then for every $u \in W_2$, there exists unique minimizer z_α of the functional $J_\alpha(z)$.*

Proof. By the variational principle the element $z_\alpha \in Q$ is a minimizer if and only if

$$(A^*Az_\alpha - A^*u, v)_2 + \alpha[z_\alpha - z_0, v] = 0, \forall v \in Q.$$

Hence,

$$(Az_\alpha, Av)_2 + \alpha[z_\alpha, v] = (A^*u, v)_2 + \alpha[z_0, v], \forall v \in Q. \tag{3.1}$$

Introduce a new scalar product $\{\cdot,\cdot\}$ in Q by

$$\{x, y\} := (Ax, Ay)_2 + \alpha[x, y], \forall x, y \in Q.$$

Since the norm in Q is stronger than the norm in W_1, then the norm $\{x\} := \sqrt{\{x,x\}}$ is equivalent to the norm $[x]$. The rest of the proof follows from the Riesz theorem. $\square$

We now prove estimate of the accuracy between the regularized solution z_α and the exact solution z^*. Such an estimate was previously established in [16] for the nonlinear case. We present now this estimate for the bounded linear operator.

Theorem 2. *Let in (2.15) $A : W_1 \to W_2$ be a bounded linear one-to-one operator. Assume that there exists a constant $\gamma > 0$ such that*

$$\|Az\|_2^2 \geq \gamma \|z\|^2, \forall z \in W_1. \tag{3.2}$$

Let z_α be the minimizer of the functional (2.14) and (2.10) holds, where the norm in $L_2(\Omega)$ is replaced with the norm in the space W_2. Then

$$||z^* - z^\alpha|| \leq \sqrt{\frac{4+\alpha^2}{4\alpha\gamma}}\ ||A||_2\ ||\delta||_2 + \frac{1}{\sqrt{\gamma}}[z^* - z_0] + \frac{\sqrt{\alpha^2 - 4\alpha}}{2\sqrt{\gamma}}[\delta].$$

Proof.

First, we write expression (3.1) for z^*:

$$(Az^*, Av)_2 + \alpha [z^*, v] = (A^*u^*, v)_2 + \alpha [z_0, v], \forall v \in Q. \tag{3.3}$$

Subtract (3.1) from (3.3) and denote $y = z^* - z_\alpha$ to get

$$(Ay, Av)_2 + \alpha [y, v] = (u^* - u, Av)_2 + \alpha [z^* - z_0, v], \forall v \in Q. \tag{3.4}$$

Using the fact that $Az^* = u^*, Az_\alpha = u$ we can rewrite above equation as

$$(Ay, Av)_2 + \alpha [y, v] = (Az^* - Az_\alpha, Av)_2 + \alpha [z^* - z_0, v], \forall v \in Q, \tag{3.5}$$

and recalling that $y = z^* - z_\alpha$ we obtain

$$(Ay, Av)_2 + \alpha [y, v] = (Ay, Av)_2 + \alpha [z^* - z_0, v], \forall v \in Q. \tag{3.6}$$

Setting here $v := y$ we have

$$(Ay, Ay)_2 + \alpha [y, y] = (Ay, Ay)_2 + \alpha [z^* - z_0, y], \forall y \in Q, \tag{3.7}$$

which can be rewritten as

$$||Ay||_2^2 + \alpha[y]^2 = (Ay, Ay)_2 + \alpha [z^* - z_0, y], \forall y \in Q. \tag{3.8}$$

First we will estimate right hand side of (3.8). Using the Cauchy-Schwarz inequality

$$ab \leq \frac{a^2}{2\varepsilon} + \frac{\varepsilon}{2} b^2, \forall \varepsilon > 0, \forall a, b, \tag{3.9}$$

we obtain

$$(Ay, Ay)_2 \leq \frac{||Ay||_2^2}{2\varepsilon} + \frac{\varepsilon}{2} ||Ay||_2^2,$$

and since $Ay = Az^* - Az^\alpha = u^* - u$ above expression can be estimated using (2.10) as

$$(Ay, Ay)_2 \leq \frac{||A||_2^2 ||\delta||_2^2}{2\varepsilon} + \frac{\varepsilon}{2} ||A||_2^2 ||\delta||_2^2,$$

and with $\alpha = 2\varepsilon$ we have

$$(Ay, Ay)_2 \leq \frac{||A||_2^2||\delta||_2^2}{\alpha} + \frac{\alpha}{4}||A||_2^2||\delta||_2^2. \tag{3.10}$$

Using again (3.9) and $\alpha = 2\varepsilon$ we obtain following estimate for the second term in the right hand side of (3.8)

$$[z^* - z_0, y] \leq \frac{[z^* - z_0]^2}{2\varepsilon} + \frac{\varepsilon}{2}[y]^2 = \frac{[z^* - z_0]^2}{\alpha} + \frac{\alpha}{4}[y]^2. \tag{3.11}$$

Estimating right hand side of (3.8) using (3.2) and collecting above estimates we have

$$\gamma||y||^2 + \alpha[y]^2 \leq ||A||_2^2||\delta||_2^2(\frac{1}{\alpha} + \frac{\alpha}{4}) + [z^* - z_0]^2 + \frac{\alpha^2}{4}[y]^2$$

which can ve rewritten as

$$||y||^2 \leq \frac{1}{\gamma}\left(\frac{4+\alpha^2}{4\alpha}\ ||A||_2^2\ |||\delta||_2^2 + [z^* - z_0]^2 + \frac{\alpha^2 - 4\alpha}{4}[y]^2\right).$$

Hence,

$$||z^* - z^\alpha|| = ||y|| \leq \frac{1}{\sqrt{\gamma}}\sqrt{\frac{4+\alpha^2}{4\alpha}}\ ||A||_2\ ||\delta||_2 + \frac{1}{\sqrt{\gamma}}[z^* - z_0] + \frac{1}{\sqrt{\gamma}}\frac{\sqrt{\alpha^2 - 4\alpha}}{2}[\delta].$$

□

4. Accuracy of the regularized solution on a locally refined meshes. It follows from Theorem 2 that it makes sense to improve the accuracy of the regularized solution via mesh refinements. Indeed, if z_k is the minimizer of the functional $J_\alpha(z)$ on the subspace M_k, then

$$\begin{aligned}\|z_k - z^*\| &\leq \|z_k - z_\alpha\| + \|z_\alpha - z^*\| \\ &\leq \|z_k - z_\alpha\| + \sqrt{\frac{4+\alpha^2}{4\alpha\gamma}}\ ||A||_2\ ||\delta||_2 + \frac{1}{\sqrt{\gamma}}[z^* - z_0] + \frac{\sqrt{\alpha^2 - 4\alpha}}{2\sqrt{\gamma}}[\delta].\end{aligned}$$

Thus, the closer z_k to z_α, the closer z_k to z^*.

From the theory of convex optimization it is known, that Lemma 2 claims existence and uniqueness of the global minimizer of the functional J_α defined in (2.14) for $z_\alpha \in Q$ such that

$$J_\alpha(z_\alpha) = \inf_{z \in Q} J_\alpha(z).$$

We also assume that the operator F is Lipschitz continuous

$$\|F(z_1) - F(z_2)\| \leq C\|z_1 - z_2\| \quad \forall z_1, z_2 \in H.$$

and it has the Frechét derivative $F'(z)$ which is also Lipschitz continuous, i.e. for certain positive constants N_1, N_2

$$\begin{aligned}\|F'(z)\| &\leq N_1, \\ \|F'(z_1) - F'(z_2)\| &\leq N_2\|z_1 - z_2\| \quad \forall z_1, z_2 \in H, \\ N_1, N_2 &= const. > 0\end{aligned} \tag{4.1}$$

We also introduce new constant $N_3 = N_3(N_1, N_2) = const. > 0$ [7, 8] such that

$$\|J'_\alpha(z_1) - J'_\alpha(z_2)\| \leq N_3\|z_1 - z_2\|, \forall z_1, z_2 \in H. \tag{4.2}$$

Theorem 3 provides an estimate of the norm $||z_k - z_\alpha||_{H^1}$ via the norm of the difference between the regularized solution z_α and its projection on the subspace M_k. Since we work in this theorem with a subspace $M_k \subset H$, we formulate this result for the functional $M_\alpha(z)$ defined in (2.13).

Let us denote by z_k the solution on the triangulation T_k and by z_α - the solution on the finally refined mesh. Then the following theorem is valid:

Theorem 3

Let $M_k \subset H$ be the subspace obtained after k mesh refinements. Suppose that all conditions of Lemma 2 are fullfiled. Let z_k be the minimizer of the Tikhonov functional (2.14) obtained after k mesh refinements. The existence of this minimizer is guaranteed by Lemma 2. Assume that the regularized solution z_α is not yet coincides with the minimizer z_k after k mesh refinements. Then there exists a constant N_3 defined by (4.2) such that the following estimate holds

$$||z_k - z_\alpha||_{H^1} \leq \frac{N_3}{\alpha} ||P_k z_\alpha - z_\alpha||_{H^1}. \tag{4.3}$$

In particular, if $P_k z_\alpha = z_\alpha$, then $z_k = z_\alpha$, which means that the regularized solution is reached after k mesh refinements.

Proof. Let z_k be a minimizer of the functional (2.13). The Lemma 2 implies that the minimizer z_k is unique. Since by the Lemma 2 the functional (2.13) is strongly convex on the space H with the strong convexity constant α, then this implies that

$$\alpha \left\| z_k - z_\alpha \right\|^2_{H^1} \leq \left(M'_\alpha (z_k) - M'_\alpha (z_\alpha), z_k - z_\alpha \right). \tag{4.4}$$

Since z_k is the minimizer of the functional (2.13), then

$$\left(M'_\alpha (z_k), y \right) = 0, \ \forall y \in M_k. \tag{4.5}$$

Next, since z_α is the minimizer on the set H, then

$$\left(M'_\alpha (z_\alpha), z \right) = 0, \ \forall z \in H.$$

Using (4.4) with the splitting

$$z_k - z_\alpha = (z_k - P_k z_\alpha) + (P_k z_\alpha - z_\alpha),$$

together with the Galerkin orthogonality principle (4.5) we obtain

$$\left(M'_\alpha (z_k) - M'_\alpha (z_\alpha), z_k - P_k z_\alpha \right) = 0 \tag{4.6}$$

and thus

$$\alpha \left\| z_k - z_\alpha \right\|^2_{H^1} \leq \left(M'_\alpha (z_k) - M'_\alpha (z_\alpha), P_k z_\alpha - z_\alpha \right). \tag{4.7}$$

Since $\left\| z_k - z_\alpha \right\|_{L_2(\Omega)} \leq ||z_k - z_\alpha||_{H^1}$, then it follows from (4.2) that

$$\left(M'_\alpha (z_k) - M'_\alpha (z_\alpha), P_k z_\alpha - z_\alpha \right) \leq N_3 ||z_k - z_\alpha||_{H^1} ||P_k z_\alpha - z_\alpha||_{H^1}.$$

Substituting above equation into (4.7) we obtain (4.3).

□

In Theorem 4 we consider the function $PM'_\alpha(z)$ instead of $M'_\alpha(z)$, where $P : L_2(\Omega) \to H$ is the operator of the orthogonal projection of $L_2(\Omega)$ onto H. We note that

$$\left(PM'_\alpha (z), f \right) = \left(M'_\alpha (z), f \right), \forall z \in H, \forall f \in H.$$

In Theorem 4 we derive a posteriori error estimates for the error in the Tikhonov functional (2.13) on the mesh obtained after k mesh refinements.

Theorem 4

Let conditions of Lemma 2 hold. Suppose that there exists minimizer $z_{\alpha,k}$ of the functional M_α on the set H and mesh T_k. Suppose also that there exists approximation of a minimizer $z_{\alpha,k,h}$ of M_α on the set H and mesh T_k. Let h_k be the maximal grid step size of the subspace M_k. Then the following approximate a posteriori error estimate for the error in the Tikhonov functional (2.13) holds

$$||M(z_{\alpha,k}) - M(z_{\alpha,k,h})||_{H^1} \leq C_I h_k \left\|M'_\alpha(z_{\alpha,k,h})\right\|_{H^1} ||z_{\alpha,k}||_{H^2} \tag{4.8}$$

Proof

By definition of the Frechét derivative we can write that on every mesh T_k

$$M(z_{\alpha,k}) - M(z_{\alpha,k,h}) = M'(z_{\alpha,k,h})(z_{\alpha,k} - z_{\alpha,k,h}) + R(z_{\alpha,k}, z_{\alpha,k,h}), \tag{4.9}$$

where by Lemma 1 $R(z_{\alpha,k}, z_{\alpha,k,h}) = O(r^2), \quad r \to 0 \ \ \forall z_{\alpha,k}, z_{\alpha,k,h} \in H$.

Now we neglect R, use the splitting

$$z_{\alpha,k} - z_{\alpha,k,h} = z_{\alpha,k} - z^I_{\alpha,k} + z^I_{\alpha,k} - z_{\alpha,k,h} \tag{4.10}$$

and the Galerkin orthogonality [14]

$$M'(z_{\alpha,k,h})(z^I_{\alpha,k} - z_{\alpha,k,h}) = 0 \ \forall z^I_{\alpha,k}, z_{\alpha,k,h} \in H_h \tag{4.11}$$

with the space of piecewise linear functions H_h for approximation of functions $z_{\alpha,k}$, to get

$$M(z_{\alpha,k}) - M(z_{\alpha,k,h}) \leq M'(z_{\alpha,k,h})(z_{\alpha,k} - z^I_{\alpha,k}), \tag{4.12}$$

where $z^I_{\alpha,k}$ is a standard interpolant of $z_{\alpha,k}$ on the mesh T_k [14]. Since $||\cdot||_{L^2} \leq ||\cdot||_{H^1}$ we have that

$$||M(z_{\alpha,k}) - M(z_{\alpha,k,h})||_{L^2} \leq ||M'(z_{\alpha,k,h})||_{L^2} ||(z_{\alpha,k} - z^I_{\alpha,k})||_{L^2} \leq ||M(z_{\alpha,k,h})||_{H^1} ||(z_{\alpha,k} - z^I_{\alpha,k})||_{H^1}, \tag{4.13}$$

where the term $||(z_{\alpha,k} - z^I_{\alpha,k})||_{H^1}$ in the right hand side of the above inequality can be estimated through the interpolation estimate with the interpolation constant C_I

$$||(z_{\alpha,k} - z^I_{\alpha,k})||_{H^1} \leq C_I h_k ||(z_{\alpha,k}||_{H^2}.$$

Substituting above estimate into (4.13) we get (4.8). $\square$

We now provide a more explicit estimate for the weaker norm $\left\|z_k - z_\alpha\right\|_{L_2(\Omega)}$. To do this, we replace in (2.13) the norm $\left\|z - z_0\right\|^2_{H^1(\Omega)}$ with the weaker norm $\left\|z - z_0\right\|^2_{L_2(\Omega)}$. As before, let h_k be the maximal grid step size of the subspace M_k.

Below in Theorems 5 and 6 we will consider the following Tikhonov functional

$$E_\alpha(z) : H \to \mathbb{R},$$

$$E_\alpha(z) = \frac{1}{2}\left\|Az - u\right\|_{L_2(\Omega)} + \frac{\alpha}{2}\left\|z - z_0\right\|^2_{L_2(\Omega)}. \tag{4.14}$$

Theorem 5. *Let $\alpha \in (0,1)$ and $A : H \to L_2(\Omega)$ be a bounded linear operator. Let z_k be the minimizer of the functional $E_\alpha(z)$ on the subspace M_k, which is obtained after k mesh refinements. Assume that the regularized solution z_α is not yet reached after k mesh refinements with the minimizer z_k. Let jump of the function z_k computed from the two neighboring elements K^+ and K^- sharing the common side S on the subspace M_k is defined by*

$$[z_k] = z^+_k - z^-_k. \tag{4.15}$$

Then there exist constants N_3, C_I defined by (4.2),(2.6), correspondingly, such that the following estimate holds

$$\|z_k - z_\alpha\|_{L_2(\Omega)} \leq \frac{C_I N_3}{\alpha} ||[z_k]||_{L_2(\Omega)}$$

Proof.
Conditions (4.2) imply that

$$\|E'_\alpha(z_k) - E'_\alpha(z_\alpha)\|_{L_2(\Omega)} \leq N_3 \|z_k - z_\alpha\|_{L_2(\Omega)} \tag{4.16}$$

with a constant $N_3 = N_3(N_1, N_2) > 0$. By (2.6)

$$\|z_\alpha - P_k z_\alpha\|_{C(K)} \leq C_I \|\nabla z_\alpha\|_{L_\infty(K)} h_k. \tag{4.17}$$

Using the Cauchy-Schwarz inequality as well as (4.16) and (4.17), we obtain from (4.3)

$$\|z_k - z_\alpha\|_{L_2(\Omega)} \leq \frac{C_I N_3}{\alpha} \|\nabla z_\alpha\|_{L_\infty(K)} h_k. \tag{4.18}$$

We can estimate $|\nabla z_\alpha|$ in following way [15]

$$|\nabla z_\alpha| \leq \frac{|[z_k]|}{h_k}$$

and substitute this estimate in (4.18) to get

$$\|z_k - z_\alpha\|_{L_2(\Omega)} \leq \frac{C_I N_3}{\alpha} \frac{\|[z_k]\|_{L_2(\Omega)}}{h_k} h_k \leq \frac{C_I N_3}{\alpha} \|[z_k]\|_{L_2(\Omega)}. \tag{4.19}$$

□

5. A posteriori error estimate for the error in the Tikhonov functional (4.14). Here we will consider the function $PE'_\alpha(z)$ instead of $E'_\alpha(z)$, where $P : L_2(\Omega) \to H$ is the operator of the orthogonal projection of $L_2(\Omega)$ onto H. In practical computations we actually compute the interpolant of $E'_\alpha(z)$ on the corresponding mesh instead of $PE'_\alpha(z)$, which are the sources of computational errors. We also note that

$$(PE'_\alpha(z), f) = (E'_\alpha(z), f), \forall z \in H, \forall f \in H.$$

In Theorem 6 we derive a posteriori error estimates for the error in the Tikhonov functional (4.14) on the mesh obtained after k mesh refinements by defining the minimizer and its approximation by $z_\alpha := z_{\alpha,k}, z_k := z_{\alpha,k,h}$, correspondingly. The proof of Theorem 6 is modification of the proof given in [11].

Theorem 6

Let conditions of Lemma 2 hold. Suppose that there exists minimizer $z_{\alpha,k}$ of the functional E_α on the set H and mesh T_k. Suppose also that there exists approximation of a minimizer $z_{\alpha,k,h}$ of E_α on the set H and mesh T_k. Then the following approximate a posteriori error estimate for the error in the Tikhonov functional (2.13) holds

$$||E(z_{\alpha,k}) - E(z_{\alpha,k,h})||_{L_2(\Omega)} \leq C_I \|E'_\alpha(z_{\alpha,k,h})\|_{L_2(\Omega)} ||[z_{\alpha,k}]||_{L_2(\Omega)} \tag{5.1}$$

Proof

By definition of the Frechét derivative we can write that on every mesh T_k

$$E(z_{\alpha,k}) - E(z_{\alpha,k,h}) = E'(z_{\alpha,k,h})(z_{\alpha,k} - z_{\alpha,k,h}) + R(z_{\alpha,k}, z_{\alpha,k,h}), \tag{5.2}$$

where by Lemma 1 $R(z_{\alpha,k}, z_{\alpha,k,h}) = O(r^2), \quad r \to 0 \quad \forall z_{\alpha,k}, z_{\alpha,k,h} \in H$.

Now we neglect R, use the splitting

$$z_{\alpha,k} - z_{\alpha,k,h} = z_{\alpha,k} - z^I_{\alpha,k} + z^I_{\alpha,k} - z_{\alpha,k,h} \tag{5.3}$$

and the Galerkin orthogonality [14]

$$E'(z_{\alpha,k,h})(z^I_{\alpha,k} - z_{\alpha,k,h}) = 0 \ \forall z^I_{\alpha,k}, z_{\alpha,k,h} \in H_h \tag{5.4}$$

with the space of piecewise linear functions H_h for approximation of functions $z_{\alpha,k}$, to get

$$E(z_{\alpha,k}) - E(z_{\alpha,k,h}) \leq E'(z_{\alpha,k,h})(z_{\alpha,k} - z^I_{\alpha,k}), \tag{5.5}$$

where $z^I_{\alpha,k}$ is a standard interpolant of $z_{\alpha,k}$ on the mesh T_k [14]. Applying interpolation estimate (2.6) to $z_{\alpha,k} - z^I_{\alpha,k}$ we get

$$||E(z_{\alpha,k}) - E(z_{\alpha,k,h})||_{L_2(\Omega)} \leq C_I \left\|E'(z_{\alpha,k,h})\right\|_{L_2(\Omega)} ||\nabla z_{\alpha,k}||_{L_\infty(\Omega)} h_k. \tag{5.6}$$

Using for $|\nabla z_\alpha, k|$ the estimate on the mesh T_k [15]

$$|\nabla z_{\alpha,k}| \leq \frac{|[z_{\alpha,k}]|}{h_k}$$

we get the following a posteriori error estimate

$$||E(z_{\alpha,k}) - E(z_{\alpha,k,h})||_{L_2(\Omega)} \leq C_I \left\|E'_\alpha(z_{\alpha,k})\right\|_{L_2(\Omega)} ||[z_{\alpha,k}]||_{L_2(\Omega)}. \tag{5.7}$$

□

Using the Theorems 5 and 6 we can now formulate our mesh refinement recommendations used in practical computations.

The First Mesh Refinement Recommendation. *Refine the mesh in neighborhoods of those points $x \in \Omega$ where the function $|E'_\alpha(z_k)(x)|$ attains its maximal values. More precisely, let $\varkappa \in (0,1)$ be the tolerance number which should be chosen in computational experiments. Refine the mesh in such subdomains of Ω where*

$$|E'_\alpha(z_k)| \geq \varkappa \max_{\overline{\Omega}} |E'_\alpha(z_k)| .$$

The Second Mesh Refinement Recommendation. *Refine the mesh in neighborhoods of those points $x \in \Omega$ where the function $|z_k(x)|$ attains its maximal values. More, precisely in such subdomains of Ω where*

$$|z_k(x)| \geq \widetilde{\varkappa} \max_{\overline{\Omega}} |z_k(x)| .$$

where $\widetilde{\varkappa} \in (0,1)$ is the number which should be chosen computationally.

6. The Adaptive Algorithm. In this section for solution of (2.7) we present adaptive algorithms which we apply in numerical examples of section 7. Our algorithms use mesh refinement recommendations of section 5. In these algorithms we also assume that the kernel in (2.7) is such that $\rho(x,y) = \rho(y-x)$. Next, using the convolution theorem we can determine the functions $z(x)$ in (2.7) and the regularized solution $z_\alpha(x)$ of (2.13), correspondingly. For example, for calculation of the function $z_\alpha(x)$ in numerical examples of section 7 we use (7.9). To reduce notations, in our algorithms we define the minimizer and its approximation $z_\alpha := z_{\alpha,k}, z_k := z_{\alpha,k,h}$, correspondingly.

In Algorithm 1 we use first mesh refinement recommendation of 5, while in Algorithm 2 are used both mesh refinement recommendations of section 5. These algorithms are successfully tested by numerical examples of section 7.

Algorithm 1

Step 0. Choose an initial mesh T_0 in Ω and obtain the numerical solution z_0 of (2.13) on T_0 using the finite element discretization of the convolution theorem (7.9). Compute the sequence $z_k, k > 0$ via following steps:

Step 1. Interpolate the given right hand side of (2.7) and the solution z_{k-1} from the mesh T_{k-1} to the mesh T_k and obtain the numerical solution z_k of (2.13) on T_k using the finite element discretization of (7.9).

Step 2. Refine the mesh T_k at all points where

$$|B'_\alpha(z_k)| \geq \beta_k \max_\Omega |B'_\alpha(z_k)|, \tag{6.1}$$

with

$$B'_\alpha(z_k) = \int\limits_\Omega \left[\int\limits_\Omega z_k(y) \left(\int\limits_\Omega \rho(x,y)\,\rho(x,s)\,dx \right) dy - \int\limits_\Omega \rho(x,s)\,u(x)\,dx \right] ds. \tag{6.2}$$

Here the tolerance number $\beta_k \in (0,1)$ is chosen by the user.

Step 3. Construct a new mesh T_{k+1} in Ω and perform steps 1-3 on the new mesh. Stop mesh refinements when $||z_k - z_{k-1}|| < \epsilon$ or $||M'_\alpha(z_k)|| < \epsilon$, where ϵ is tolerance chosen by the user.

Algorithm 2

Step 0. Choose an initial mesh T_0 in Ω and obtain the numerical solution z_0 of (2.13) on T_0 using the finite element discretization of the convolution theorem (7.9). Compute the sequence $z_k, k > 0$ via following steps:

Step 1. Interpolate the given right hand side of (2.7) and the solution z_{k-1} from the mesh T_{k-1} to the mesh T_k and obtain the numerical solution z_k of (2.13) on T_k using the finite element discretization of (7.9).

Step 2. Refine the mesh T_k at all points where

$$|B'_\alpha(z_k)| \geq \beta_k \max_\Omega |B'_\alpha(z_k)| \tag{6.3}$$

with $B'_\alpha(z_k)$ defined by (6.2), and where

$$|z_k(x)| \geq \widetilde{\varkappa_k} \max_{\overline{\Omega}} |z_k(x)|. \tag{6.4}$$

Here the tolerance numbers $\beta_k, \widetilde{\varkappa_k} \in (0,1)$ are chosen by the user.

Step 3. Construct a new mesh T_{k+1} in Ω and perform steps 1-3 on the new mesh. Stop mesh refinements when $||z_k - z_{k-1}|| < \epsilon$ or $||M'_\alpha(z_k)|| < \epsilon$, where ϵ is tolerance chosen by the user.

Remarks

We note that the choice of the tolerance numbers $\beta_k, \widetilde{\varkappa_k}$ in (6.2), (6.4) depends on the concrete values of $\max_\Omega |B'_\alpha(z_k)|$ and $\max_{\overline{\Omega}} |z_k(x)|$, correspondingly. If we would choose $\beta_k, \widetilde{\varkappa_k}$ very close to 1 then we would refine the mesh in very narrow region of the computational domain Ω, and if we will choose $\beta_k, \widetilde{\varkappa_k} \approx 0$ then almost all mesh of the domain Ω will be refined what is unsatisfactory. Thus, the values of the numbers $\beta_k, \widetilde{\varkappa_k}$ should be chosen in optimal way. Our numerical tests show that the choice of $\beta_k, \widetilde{\varkappa_k} = 0.5$ is almost optimal one, however, it can be changed during the iterations from one mesh to other.

We also note that we neglect the computation of the regularization term in a posteriori error indicator (6.2) since this term is very small and does not affects on the refinement procedure. However, this term is included in the minimization procedure of the Tikhonov's functional (2.13).

7. Numerical studies of the adaptivity technique in microtomography. In all our tests of this section we consider the problem of the two-dimensional reconstruction of the backscattered signal in microtomography [4, 5]. This method allows nondestructive layer-by-layer image restoration of micro and nanostructures, for example, reconstruction of integral microschemes.

Backscattered signal in Test 3 of subsection 7.3 is generated by the microtomograph developed by professor Eduard Rau at Moscow Lomonosov State University. This device is based on the electron microscope working in the backscattering electron mode. Scheme of this device is presented on Figure 7.1. As soon as images are obtained by the device of Figure 7.1, they can be improved by mathematical methods. It is well known, that in mathematics the problem of the image restoration in microtomography consists in solution of the Fredholm integral equation of the first kind which is ill-posed problem. Usual method for solution of this equation in two and three dimensions is minimization of the Tikhonov functional (2.13) in some bounded domain $\Omega \subset \mathbb{R}^n, n = 2, 3$ using deconvolution algorithm on the uniform mesh [4, 5].

In the numerical tests of this section we show examples of the image restoration in microtomography using adaptive finite element method with piecewise linear functions on a locally refined meshes. We present numerical studies of the adaptive algorithms of section 6 on the computationally simulated data (Tests 1,2 in subsection 7.3) and on the experimental data (Test 3 in subsection 7.3). In Test 2 of subsection 7.3) we also compare results obtained by the uniform deconvolution algorithm of [4, 5] with the adaptivity technique of this paper.

7.1. Experimental setup. The scheme of the data collection is presented in Figure 7.1. The method of the collecting backscattered data consists on the analysis of the energy loss of the backscattered electrons. The energy filtration E_0 allows us to fix only the electrons backscattered from the depth t corresponding to the scattering energy E_s. To define the intensity of the backscattered electron signal we use following expression

$$I_s = C_0 \eta(k x_{\eta c}) {E_s}^2 (1 - \frac{2.1 x_{\eta c}}{R_0}). \tag{7.1}$$

Here, $\eta(k x_{\eta c})$ is the scattering coefficient, k is the density of the material, $x_{\eta c} = 0.5 C_1(kZ) {E_0}^2 Z^{-0.333} e^{-0.022Z}$ is the most probable depth of backscattering electrons, $R_0 = C_1(kZ){E_0}^2$ - the total depth of the penetration of the electrons inside the material of the target.

The energy E_s depends on the depth $x_{\eta c}$ and the energy E_0 through the empirical expression

$$\frac{E_s}{E_0} = \big(1 - \frac{2.7 x_{\eta c}}{R_0}\big). \tag{7.2}$$

Using (7.2) we can conclude that by appropriately selecting of energies E_0 and E_s we can tune the device on the some depth t of the target and get spatial information about the structure of the object under investigation. However, the method of producing images using the device of Figure 7.1 has following problems:

- Finite radius and nonlinear arrangement of the current density in the electron ray can significantly blur or erosion images.
- Nonlinear arrangement of the energy in the electron ray on some depth of the penetration can occur in imposition of the layers lying close to each other.
- Imposition of the layers lying far from each other are defined by the features of the structure of the object under investigation.

In this paper we show reconstruction results for the first problem. Namely, we will restore blurred images using adaptive finite element method. Blurring of images can be explained by the fact that the finite radius of the electron probe leads to the situation, when every point of the layer under investigation becomes some spot on the image of this layer.

Let us denote by r_0 the known radius of the primary electron beam outside the target. The radius r of the electron probe on the penetration depth t can be represented using the empiric formula

$$r(t)^2 = r_0^2 + 0.625 \left(\frac{Z}{E_0}\right)\left(\frac{\rho}{A}\right)^{0.5} t^{1.5}, \tag{7.3}$$

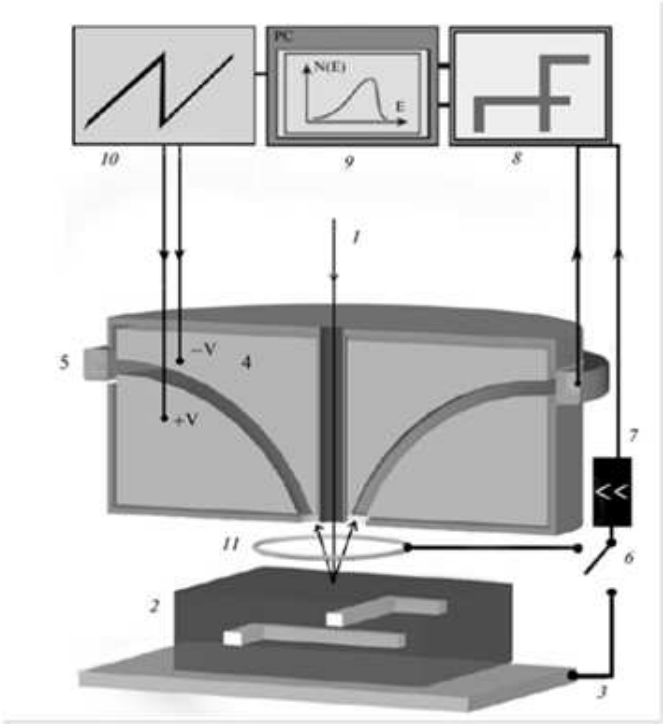

Fig. 7.1: The working principle of the device. Primary monokinetic electron beam 1 with the particle energy E_0 falls normally on the plane surface of the object under investigation 2. Object is located on the metallic substrate 3 for grounding. Part of the primary beam is backscattered from the different depths of the object and comes to the spectrometer 4, setted on some energy E_s, or to the detector of electrons 11 depending on the position of the swich 6. Part of the backscattered ray, which corresponds to the energy E_s, falls through the spectrometer on the detector of electrons 5. From the detector 5 or 11 the signal, which is proportional to the number of electrons and their energy, comes to the videocontrol device 8 or to the personal computer 9. In the case when the detector of electrons 11 is turned on, the signal comes to these devices through the charge-sensitive preamplifier 7. To reduce the noise, the spectrometer is fed with a sawtooth voltage power supply unit 10.

where Z and A are the atomic number and the atomic weight, respectively. Here, r and t are expressed in [cm], E_0 - in [keV], the current dencity of the material of the target ρ - in [g/cm^3].

The arrangement of the current dencity in the cross section of the electron probe can be represented as a Gauss arrangement [5]. This arrangement transforms on the depth t with the scaling parameter $r(t)$ defined by (7.3). In fact, this is a radius of the electron probe. Thus, the arrangement of the current density can be calculated using the expression

$$\rho(r') = \frac{1}{2\pi r^2} \exp(-\frac{r'^2}{2r^2}) \tag{7.4}$$

or in the Cartesian coordinate system - using the formula

$$\rho(x, y) = \frac{1}{2\pi r^2} \exp(-\frac{x^2 + y^2}{2r^2}). \tag{7.5}$$

The image is formed then line by line through the integral measuring of the intensity of backscattered electron signal. The measured intensity saved into the point of a plane image, which corresponds to the position of the electron probe.

7.2. Statement of the problem. Let us introduce the Cartesian coordinate system xOy in the plane of the layer under investigation. Let $z(x,y)$ be the scattering coefficient at the point with coordinates (x,y). Let $\xi O\eta$ be other Cartesian coordinate system which is defined in the plane of the image. Without loss of generality we can assume, that this system is equivalent to the system xOy. If the electron probe is located at some point (ξ,η) of the layer under investigation, then the intensity at this point is proportional to the number of electrons backscattered from the object.

Let Ω will be bounded domain representing the object to be investigated which is decomposed into N small rectangular subdomains ω_i such that $\Omega = \cup_{i=1}^{N}\omega_i, \quad \omega_i \cap \omega_j = 0 \ \ \forall i \neq j$. Let subdomains ω_i have sizes dx, dy such that $\omega_i = dx \times dy$. We assume a constant scattering coefficient $z(x,y)$ inside every subdomain ω_i. Then the backscattered signal from the domain ω_i at the point (ξ,η) is defined by the formula

$$u(\xi,\eta) = \int\limits_{\omega_i} z(x,y)\rho(x-\xi,y-\eta)dxdy. \tag{7.6}$$

Taking the sum over all subdomains $\omega_i \subset \Omega$ we get expression for the backscattered signal $u(\xi,\eta)$ at the point (ξ,η) in the whole domain Ω

$$u(\xi,\eta) = \int\limits_{\Omega} z(x,y)\rho(x-\xi,y-\eta)dxdy. \tag{7.7}$$

Inverse problem

Inverse problem consists in the calculating of the intensity arrangement $z(x,y)$ by using known values of the functions $u(\xi,\eta)$ and $\rho(x-\xi,y-\eta)$ in (7.7).

To solve the inverse problem we minimize the Tikhonov functional (2.13) in the form

$$M_\alpha(z) = ||\int\limits_{\Omega} \rho(x-\xi,y-\eta)z(x,y)dxdy - u(\xi,\eta)\|^2_{L_2(\Omega)} + \alpha\|z(x,y)\|^2_{H^1}. \tag{7.8}$$

Using the convolution theorem we can easily obtain the formula of the minimizer $z_\alpha(x,y)$ of the functional (7.8)

$$z_\alpha(x,y) = \int_\Omega e^{-i(\lambda x+\nu y)}\frac{P^*(\lambda,\nu)U(\lambda,\nu)}{|P(\lambda,\nu)|^2+\alpha(1+\lambda^2+\nu^2)^2}d\lambda d\nu \tag{7.9}$$

where functions U and P are the Fourier images of the functions u and ρ, respectively.

In [5, 18] the solution of the equation (7.7) was found on uniform grids on the spaces H^1 and $VH(B)$ (the space of functions with bounded total variation). The best reconstruction result was obtained using the bounded total variation functions when for the first approximation was taken the result obtained on space H^1. Our computational tests of section 7.3 show the better stability for the adaptive method then methods of [5, 18].

7.3. Results of the reconstruction using adaptive finite element method.

7.3.1. Test 1-a). The goal of this test was to restore the image presented on the Figure 7.2-a). The image of Figure 7.2-a) is simulation of the function $u(\xi,\eta)$ in (7.6) for the data from the electron microscope with the smearing parameter $r' = 0.188$ mkm in (7.4). Area of the image of Figure 7.2-a) is $\Omega = 3.4813$ mkm. For restoration of the image of Figure 7.2-a) we apply the first adaptive algorithm of section 6. First, we compute z_0 using the finite element discretization of (7.9) with the regularization parameter $\alpha = 3e10-07$ in (7.8) on the coarse mesh presented in Figure 7.2-g). Let us define the function

$$B'_\alpha(z_k) = \int\limits_\Omega \left[\int\limits_\Omega z_k(y)\left(\int\limits_\Omega \rho(x-\xi,y-\eta)\,\rho(x-\xi,s-\eta)\,dx\right)dy - \int\limits_\Omega \rho(x-\xi,s-\eta)\,u(x)\,dx\right]ds, \tag{7.10}$$

where Ω is our two-dimensional domain.

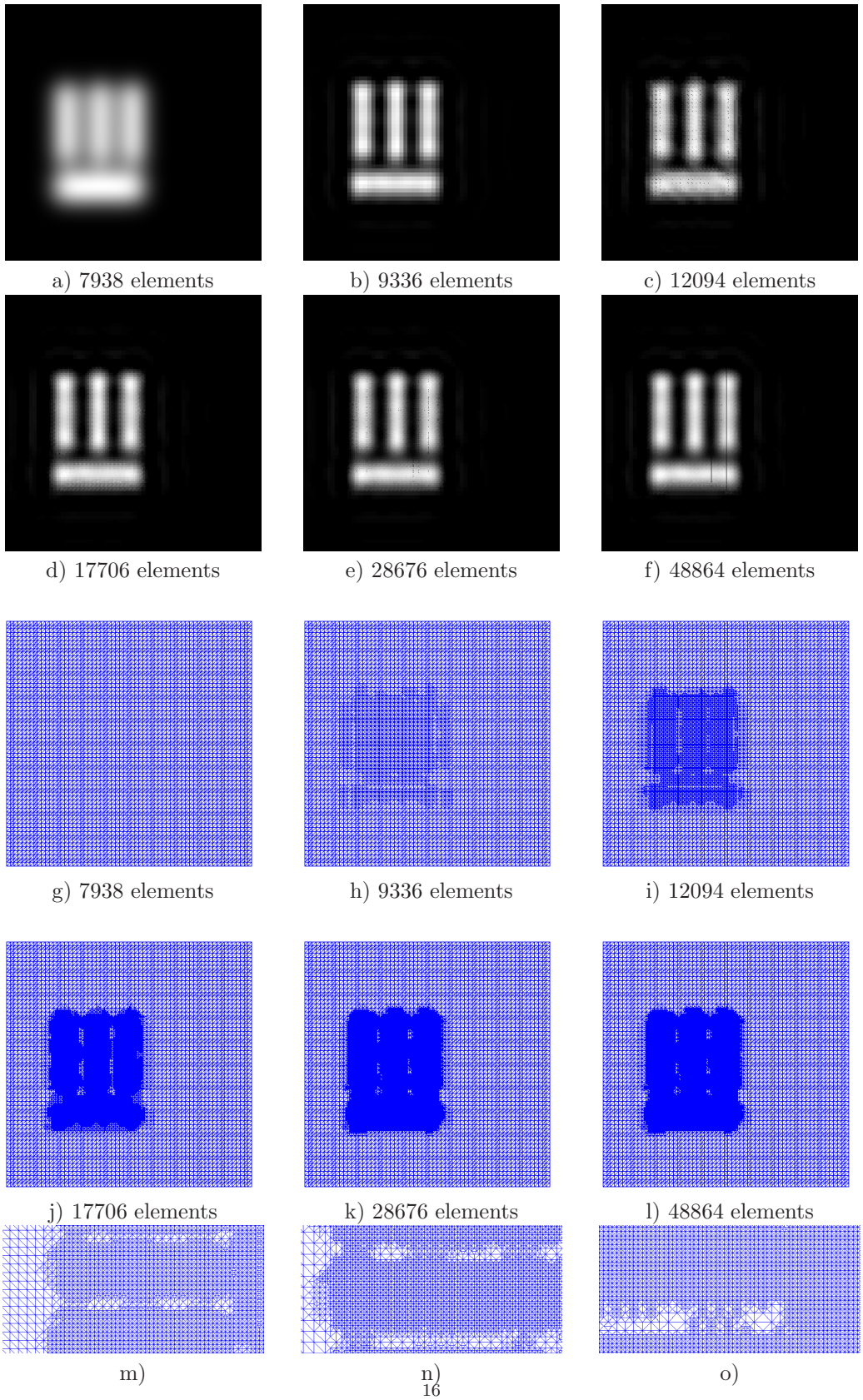

a) 7938 elements b) 9336 elements c) 12094 elements

d) 17706 elements e) 28676 elements f) 48864 elements

g) 7938 elements h) 9336 elements i) 12094 elements

j) 17706 elements k) 28676 elements l) 48864 elements

m) n) o)

Fig. 7.2: Test 1-a). Image restoration of the simulated data from the the electron microscope. On a) we present simulated measured data. On b)-f) we show the results of the image restoration on different adaptively refined meshes using the algorithm of section 6. Adaptively refined meshes corresponding to the images on b)-f) are presented on h)-l). Enlarged parts of the refined meshes on j), k), l) are presented on m), n), o), respectively.

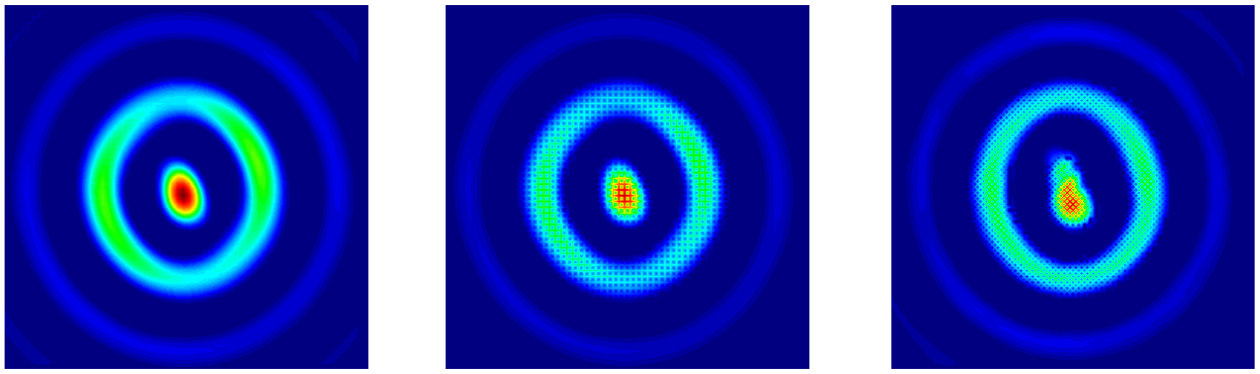

a) 7938 elements b) 9604 elements c) 12798 elements

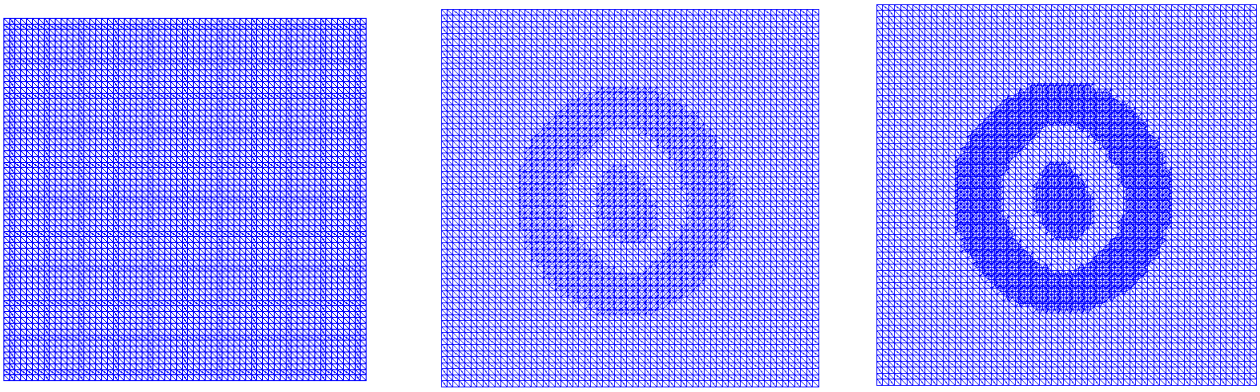

d) 7938 elements e) 9604 elements f) 12798 elements

Fig. 7.3: Test 1-b). Image restoration of the simulated data from the the electron microscope. On a) we present simulated measured data. On b)-f) we show the results of the image restoration on different adaptively refined meshes using the algorithm of section 6. Adaptively refined meshes corresponding to the images on b)-c) are presented on e)-f).

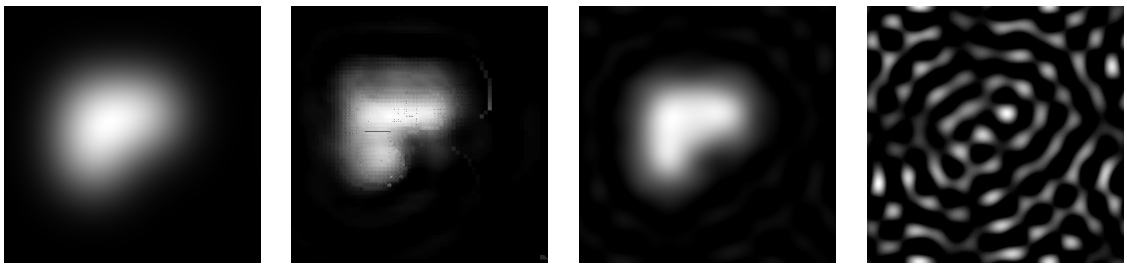

a) b) c) d)

Fig. 7.4: Test2. Efficiency of the application of the adaptive mesh refinement for calculation of the deconvolution function z_α given by (7.9). a) Simulated measured data. b) Computed deconvolution result of the function z_α on the adaptively refined mesh with $\alpha = 2e10 - 7$. c),d) Computed deconvolution result of the function z_α on the uniform mesh with the regularization parameters $\alpha = 0.01$ and $\alpha = 2e10 - 7$, respectively.

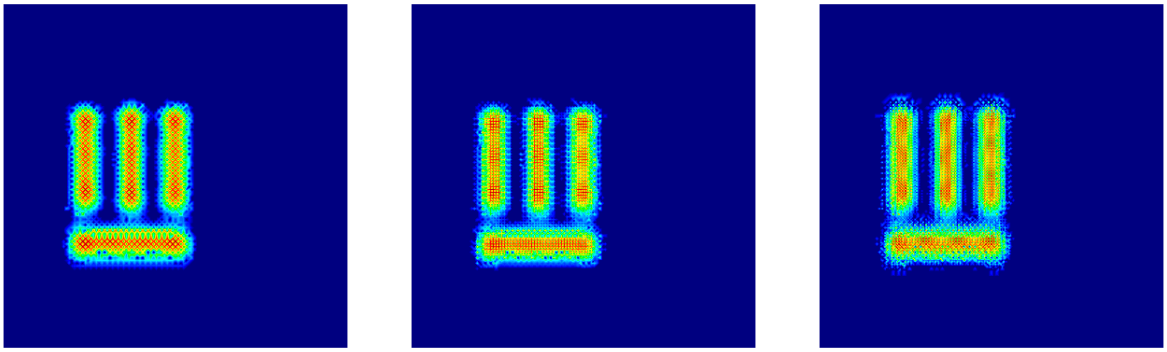

a) 17706 elements b) 28676 elements c) 48864 elements

Fig. 7.5: Test 1-a). Image restoration on the simulated data. Presentation of the results in color scale. Figures a),b),c) corresponds to the Figures 7.2-d),e),f).

We refine the mesh in all subdomains where the gradient of the function $B'_\alpha(z_k)$ attains its maximal values, or where

$$|B'_\alpha(z_k)| \geq \beta_k \max_{\Omega} |B'_\alpha(z_k)| \tag{7.11}$$

with $\beta_k = 0.5$. Next, we perform all steps of the first adaptive algorithm of section 6 until the desired tolerance $||z_k - z_{k-1}|| < \epsilon$ with $\epsilon = 10e-05$ is achieved, or the computed L_2- norms of the differences $||z_k - z_{k-1}||$ are started abruptly grow.

Figures 7.2-b)-f) show results of the reconstruction of the function $z(x,y)$ in (7.6) on the adaptively refined meshes presented in Figures 7.2-h)-l). We observe that on the fifth refined mesh corresponding to the Figure 7.2-l) we obtain the best restoration results. Since the computed L_2- norms $||z_k - z_{k-1}||$ are started abruptly grow after the fifth refinement of the initial mesh we conclude that the restoration image for the function $z(x,y)$ of the Figure 7.2-f) is the resulting one.

7.3.2. Test 1-b). This test is similar to the previous one only the goal was to restore the image presented on the Figure 7.3-a). The image of Figure 7.3-a) is simulation of the function $u(\xi,\eta)$ in (7.6) for the data from the electron microscope with the smearing parameter $r' = 0.188$ mkm in (7.4). For restoration of the image of Figure 7.3-a) we apply the second adaptive algorithm of section 6 with both mesh refinement recommendations of Section 5. Figures 7.3-b)-c) show results of the reconstruction of the function $z(x,y)$ in (7.6) on the adaptively refined meshes presented in Figures 7.3-e)-f). Stopping criterion for mesh refinements is the same as in the Test 1-a).

We observe that on the second refined mesh corresponding to the Figure 7.3-f) we obtain the best restoration results. Since the computed L_2- norms $||z_k - z_{k-1}||$ are started abruptly grow after the second refinement of the initial mesh we conclude that the restoration image for the function $z(x,y)$ of the Figure 7.3-c) is the resulting one.

7.3.3. Test 2. The goal of this test is to present the efficiency and robustness of the applying of the adaptive mesh refinement for calculating of the deconvolution function z_α given by (7.9).

On Figure 7.4-a) we present simulation of the real image measured by the electron microscope with the smearing parameter $r' = 0.0612$ mkm in (7.4) and with the area of the image 6.963 mkm. On Figure 7.4-b) we present computed result of the deconvolution of the function z_α on the adaptively refined mesh using the first adaptive algorithm of section 6. In this example the regularization parameter in Tikhonov functional is chosen $\alpha = 2e10 - 7$.

Figure 7.4-c) shows computed result of the deconvolution of the function z_α on the uniform mesh with the regularization parameter $\alpha = 0.01$. Figure 7.4-d) shows that the image blows up on the uniform mesh when taking the regularization parameter $\alpha = 2e10 - 7$ in the Tikhonov functional.

Comparing results of Figures 7.4 we can conclude that the computed deconvolution function z_α on the adaptively refined mesh of the Figure 7.4-b) is better then the corresponding function on the uniform mesh of the Figure 7.4-c). We observe, that this function blows up on the uniform mesh with the regularization parameter taken the same as in the adaptive algorithm, compare results of Figure 7.4-b) with the Figure 7.4-d). This test points out towards the robustness of using the adaptive algorithm for image restoration problems.

7.3.4. Test 3. In this test our goal was to restore image of Figure 7.6-a) which represents the part of the planar microscheme obtained from the experimentally measured data by microtomograph [4, 5]. This image was measured on the depth 0.9 μm of the microscheme with the smearing parameter $r' = 0.149$ mkm in (7.4). Real area of the image of Figure 7.6-a) is $\Omega = 16.963$ mkm. For restoration of the image of Figure 7.6-a) we apply the first adaptive algorithm of section 6. First, we compute z_0 using the finite element discretization of (7.9) with the regularization parameter $\alpha = 2e10 - 07$ in (7.8) on the coarse mesh presented in Figure 7.6-g). Then we refine the mesh in all subdomains where the gradient of (7.10) attains its maximal values by choosing $\beta_k = 0.5$ in (7.11). Next, we perform all steps of the adaptive algorithm until the desired tolerance $||z_k - z_{k-1}|| < \epsilon$ with $\epsilon = 10e - 05$ is achieved or the computed L_2- norms of the differences $||z_k - z_{k-1}||$ are started abruptly grow.

Figures 7.6-b)-f) show results of the reconstruction on the adaptively refined meshes which are presented in Figures 7.6-h)-l). Using this Figure we observe that on the fifth refined mesh corresponding to the Figure7.6-l) we obtain the best restoration results. Since the computed L_2- norms $||z_k - z_{k-1}||$ are started abruptly grow after the fifth refinement of the initial mesh we conclude that the restoration image of the Figure 7.6-f) is the resulting one.

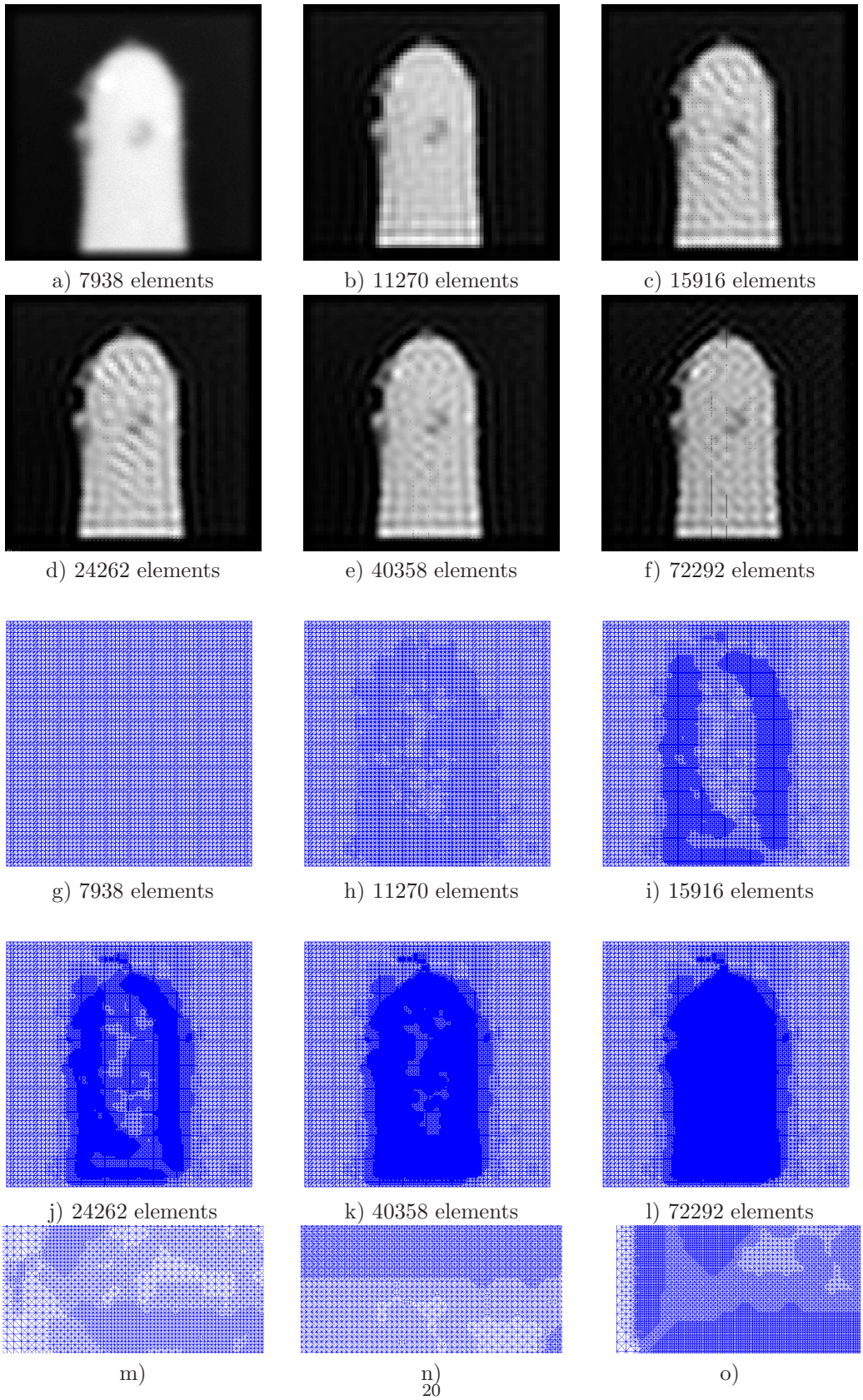

Fig. 7.6: Test 3. Reconstructed images from the experimental backscattering data obtained by the microtomograph [4, 5]. On a) we present the real measured signal on the part of the planar microscheme obtained by microtomograph on the depth 0.9 μm. On b)-f) we show results of the image restoration presented on a) on different adaptively refined meshes using the algorithm of section 6. Adaptively refined meshes corresponding to the images on b)-f) are presented on h)-l). Enlarged parts of refined meshes on j), k), l) are presented on m), n), o), respectively.

Acknowledgments

This research was supported by the Swedish Research Council, the Swedish Foundation for Strategic Research (SSF) in Gothenburg Mathematical Modelling Centre (GMMC) and by the Swedish Institute, Visby Program. The first author acknowledges also the Russian Foundation For Basic Research, the grant RFFI 11-01-00040.

REFERENCES

[1] A.V.Goncharsky, A.M.Cherepashchuk, A.G.Yagola. Ill-posed problems of astrophysics. -Moscow, Nauka, 1985, p. 1-352 (in Russian).

[2] Yu.A.Basistov, A.V.Goncharsky, E.E.Lekht, A.M.Cherepashchuk, A.G.Yagola. Application of the regularization method for increasing of the radiotelescope resolution power, *Astron. zh.*, 56, N 2, 1979, p. 443-449 (in Russian).

[3] V.D.Rusov, Yu.F.Babikova, A.G.Yagola. Image restoration in electronic microscopy autoradiography of surfaces. Moscow, Energoatomizdat, 1991, p. 1-216 (in Russian).

[4] A.G. Yagola, N.A. Koshev. Restoration of smeared and defocused color images, *Numerical Methods and Programming*, v. 9, 2008, pp. 207-212 (in Russian).

[5] N.A. Koshev, N.A. Orlikovsky, E.I. Rau, A.G. Yagola. Solution of the inverse problem of restoring the signals from an electronic microscope in the backscattered electron mode on the class of bounded variation functions, *Numerical Methods and Programming*, v.12, 2011, pp. 362-367 (in Russian).

[6] A.V.Bolotina, F.A.Lukyanov, E.I. Rau, R.A. Sennov, A.G.Yagola. Energy spectra of the electrons backscattered of the massive targets, *Vestnik Moskovskogo Universiteta, Section 3:Physics, Astronomy*, vol.5 pp.30-32, 2009.

[7] A. B. Bakushinsky, M. Y. Kokurin, A. Smirnova, *Iterative methods for ill-posed problems*, Walter de Gruyter GmbH&Co., 2011.

[8] A.B. Bakushinsky, *A posteriori* error estimates for approximate solutions of irregular operator equations, *Doklady Mathematics*, 83, 1-2, 2011.

[9] L. Beilina, M.V. Klibanov and M.Yu. Kokurin, Adaptivity with relaxation for ill-posed problems and global convergence for a coefficient inverse problem, *Journal of Mathematical Sciences*, 167, 279-325, 2010.

[10] L. Beilina and M.V. Klibanov, *A posteriori* error estimates for the adaptivity technique for the Tikhonov functional and global convergence for a coefficient inverse problem, *Inverse Problems,* 26**,** 045012, 2010.

[11] L. Beilina, M. V. Klibanov and A. Kuzhuget, New a posteriori error estimates for adaptivity technique and global convergence for a hyperbolic coefficient inverse problem, *Journal of Mathematical Sciences,* 172, 449-476, 2011.

[12] L.Beilina, M.V.Klibanov, Reconstruction of dielectrics from experimental data via a hybrid globally convergent/adaptive inverse algorithm, *Inverse Problems*, 26, 125009, 2010.

[13] S. C. Brenner and L. R. Scott, *The Mathematical Theory of Finite Element Methods* (2nd edn), Springer-Verlag, New York, 2002.

[14] K. Eriksson, D. Estep and C. Johnson, *Calculus in Several Dimensions*, Springer, Berlin, 2004.

[15] C. Johnson and A. Szepessy, Adaptive finite element methods for conservation laws based on a posteriori error estimation, *Comm. Pure Appl. Math.*, 48, 199–234, 1995.

[16] M.V. Klibanov, A.B. Bakushinsky and L. Beilina, Why a minimizer of the Tikhonov functional is closer to the exact solution than the first guess, *J. Inverse and Ill-Posed Problems*, 19, 83-105, 2011.

[17] A.N. Tikhonov, A.V. Goncharsky, V.V. Stepanov and A.G. Yagola, *Numerical Methods for the Solution of Ill-Posed Problems*, London: Kluwer, London, 1995.

[18] N.A. Koshev, F.A. Luk'anov, E.I. Rau, R.A. Sennov, and A.G. Yagola. Increasing Spatial Resolution in the Backscattered Electron Mode of Scanning Electron Microscopy, *Bulletin of the Russian Academy of Sciences. Physics.* v. 75, No. 9, pp. 1181-1184. Allerton Press, 2011.